Resource

TRANSPARENT PROCESS

THE EMBO JOURNAL

In situ CRISPR-Cas9 base editing for the development of genetically engineered mouse models of breast cancer

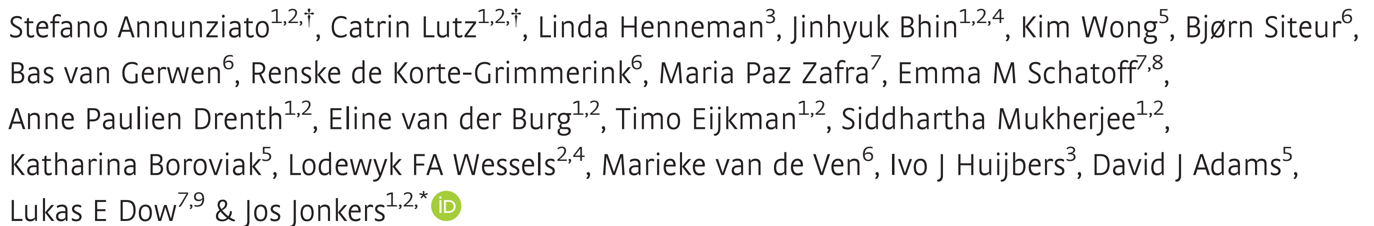

Stefano Annunziato[1,2,†], Catrin Lutz[1,2,†], Linda Henneman[3], Jinhyuk Bhin[1,2,4], Kim Wong[5], Bjørn Siteur[6], Bas van Gerwen[6], Renske de Korte-Grimmerink[6], Maria Paz Zafra[7], Emma M Schatoff[7,8], Anne Paulien Drenth[1,2], Eline van der Burg[1,2], Timo Eijkman[1,2], Siddhartha Mukherjee[1,2], Katharina Boroviak[5], Lodewyk FA Wessels[2,4], Marieke van de Ven[6], Ivo J Huijbers[3], David J Adams[5], Lukas E Dow[7,9] & Jos Jonkers[1,2,*]

Abstract

Genetically engineered mouse models (GEMMs) of cancer have proven to be of great value for basic and translational research. Although CRISPR-based gene disruption offers a fast-track approach for perturbing gene function and circumvents certain limitations of standard GEMM development, it does not provide a flexible platform for recapitulating clinically relevant missense mutations *in vivo*. To this end, we generated knock-in mice with Cre-conditional expression of a cytidine base editor and tested their utility for precise somatic engineering of missense mutations in key cancer drivers. Upon intraductal delivery of sgRNA-encoding vectors, we could install point mutations with high efficiency in one or multiple endogenous genes *in situ* and assess the effect of defined allelic variants on mammary tumorigenesis. While the system also produces bystander insertions and deletions that can stochastically be selected for when targeting a tumor suppressor gene, we could effectively recapitulate oncogenic nonsense mutations. We successfully applied this system in a model of triple-negative breast cancer, providing the proof of concept for extending this flexible somatic base editing platform to other tissues and tumor types.

Keywords base editing; breast cancer; CRISPR-Cas9; genetically engineered mouse models; intraductal injections

Subject Categories Cancer; Synthetic Biology & Biotechnology

DOI 10.15252/embj.2019102169 | Received 3 April 2019 | Revised 29 November 2019 | Accepted 2 December 2019

The EMBO Journal (2020) e102169

Introduction

Genetic sequencing studies defined a catalog of somatic alterations in breast cancer (Nik-Zainal *et al*, 2016). However, deconvoluting the molecular complexity of breast tumors requires tractable and informative genetic models. Genetically engineered mouse models (GEMMs) represent the most sophisticated models of human breast cancer, as they simulate the stepwise progression of a healthy mammary cell to hyperplasia and invasive disease in the context of a native stromal compartment and in the presence of a functional immune system. However, the amount of resource and time required to derive new GEMM lines and to incorporate new mutant alleles within complex genotypes limits the experimental throughput.

In recent years, CRISPR-Cas9 genome editing has revolutionized gene function studies. The unprecedented ease with which endogenous loci can be perturbed with this method has opened a myriad of possibilities in terms of *in vivo* modeling of alterations observed in human malignancies. We previously showed that CRISPR-mediated somatic engineering of the mammary gland is feasible and effective using intraductal injection of lentivirally encoded sgRNAs in female Cas9 knock-in mice (Annunziato *et al*, 2016). With this method, double-strand DNA breaks (DSB) can be generated *in situ* at a

1 Division of Molecular Pathology, The Netherlands Cancer Institute, Amsterdam, The Netherlands
2 Cancer Genomics Netherlands, The Netherlands Cancer Institute, Amsterdam, The Netherlands
3 Transgenic Core Facility, Mouse Clinic for Cancer and Aging (MCCA), The Netherlands Cancer Institute, Amsterdam, The Netherlands
4 Division of Molecular Carcinogenesis, The Netherlands Cancer Institute, Amsterdam, The Netherlands
5 Wellcome Trust Sanger Institute, Cambridge, UK
6 Preclinical Intervention Unit, Mouse Clinic for Cancer and Aging (MCCA), The Netherlands Cancer Institute, Amsterdam, The Netherlands
7 Division of Hematology and Medical Oncology, Department of Medicine, Sandra and Edward Meyer Cancer Center, Weill Cornell Medicine, New York, NY, USA
8 Weill Cornell/Rockefeller/Sloan Kettering Tri-I MD-PhD Program, New York, NY, USA
9 Department of Biochemistry, Sandra and Edward Meyer Cancer Center, Weill Cornell Medicine, New York, NY, USA
*Corresponding author. Tel: +31 020 512 2000; E-mail: j.jonkers@nki.nl
†These authors contributed equally to this work

© 2020 The Authors

precise target location in the genome of mammary cells, and DNA repair processes such as non-homologous end joining (NHEJ) can result in the formation of insertions or deletions (indels), which may interrupt the open reading frame (ORF) and typically lead to gene disruption. This platform has proven instrumental in the assessment of the collaborative role of putative tumor suppressors in multiple breast cancer subtypes, including invasive lobular carcinoma (ILC; Kas *et al*, 2017) and triple-negative breast cancer (TNBC; Annunziato *et al*, 2019). However, it is mostly applicable for probing the effects of complete loss of function of a candidate gene, whereas the most common disease-associated mutations seen in human breast cancer are point mutations (Nik-Zainal *et al*, 2016), which can have more subtle consequences. Therefore, a way for rapidly installing precise mutations in the mouse mammary gland would provide a significant technological advance.

Base editing is a new genome editing technology which allows for the precise alteration of a DNA sequence without direct DSB formation (reviewed in Rees & Liu, 2018). The most characterized base editors, cytidine base editors (CBEs), are chimeric fusions composed of a nuclease-defective Cas9 tethering a cytidine deaminase to specific DNA sequences to produce C-to-T transitions within defined windows of the protospacer.

In this study, we developed a knock-in mouse model for Cre-conditional expression of the BE3 cytidine base editor (Komor *et al*, 2016) in the mammary gland. We injected these mice with lentiviral vectors encoding one or multiple arrayed sgRNAs designed to install missense or nonsense mutations at one or multiple endogenous loci. This platform enabled rapid modeling of oncogenic variants and allelic series of oncogenes and tumor suppressors *in vivo*, and to test their contribution to tumorigenesis in a model of TNBC.

Results

Although BRCA1-associated TNBC is primarily a copy-number driven disease, mutations in *TP53* and the PI3K/AKT pathway are, together with *MYC* copy-number variations, the most prominent aberrant events in these tumors (Annunziato *et al*, 2019). We previously employed the *WapCre;Brca1*$^{F/F}$*;Trp53*$^{F/F}$*;Col1a1*$^{invCAG\text{-}Cas9/+}$ (WB1P-Cas9) mouse model of BRCA1-associated TNBC. In this model, mammary-specific expression of Cre induces inactivation of BRCA1 and p53 and concomitant expression of Cas9. We could use intraductal injection of Lenti-sgRNA-*Myc* lentiviral vectors in WB1P-Cas9 mice to test how disruption of specific genes (e.g., *Pten* or *Rb1*) collaborates with MYC overexpression in BRCA1-associated TNBC formation (Annunziato *et al*, 2019).

In order to model missense mutations rather than gene disruptions *in situ*, we generated a mouse model with conditional expression of the base editor BE3 in the mammary gland. The BE3 CBE is a hybrid protein that comprises the *Streptococcus pyogenes* Cas9 nickase (SpCas9^{D10A}) fused with the rat APOBEC1 cytidine deaminase and a uracil glycosylase inhibitor (UGI) domain (Komor *et al*, 2016). Upon delivery of an sgRNA, the Cas9 moiety of BE3 engages with the genomic target site and positions the deaminase enzyme at its 5′ end, where C-to-T transitions may be generated within a small 4–5 nucleotide window. *WapCre;Brca1*$^{F/F}$*;Trp53*$^{F/F}$*;Col1a1*$^{invCAG\text{-}BE3/+}$ (WB1P-BE3) mice were generated using our previously established GEMM-ESC pipeline (Huijbers *et al*, 2014). In brief, a Cre-conditional *invCAG-BE3* allele (Appendix Fig S1A) was introduced into the *Col1a1* locus of embryonic stem cells (ESCs) derived from *WapCre;Brca1*$^{F/F}$*;Trp53*$^{F/F}$ (WB1P) mice and chimeric mice were produced by blastocyst injection of the modified cells. High-quality male chimeras were then back-crossed with *Brca1*$^{F/F}$*;Trp53*$^{F/F}$ females to generate the experimental cohort. In this WB1P-BE3 model, female mice spontaneously developed mammary tumors with a median latency of 195 days ($n = 17$; Appendix Fig S1B), which is comparable to the previously reported latency of WB1P females (198 days, Annunziato *et al*, 2019). Similarly to WB1P tumors, WB1P-BE3 tumors were poorly differentiated carcinomas with a solid growth pattern, negative for estrogen receptor (ER), progesterone receptor (PR), and human epidermal growth factor receptor 2 (HER2) (Fig EV1A). To confirm that tumors from this new mouse model recapitulate the basal-like phenotype typical for WB1P tumors and for human BRCA1-associated breast cancer (Annunziato *et al*, 2019), we performed RNA sequencing on 6 WB1P-BE3 tumors and compared their expression profile to tumors from published mouse models of luminal (*WapCre;Cdh1*$^{F/F}$*;Pten*$^{F/F}$, WEP) and basal-like (*K14Cre;Brca1*$^{F/F}$*;Trp53*$^{F/F}$, KB1P; *WapCre;Brca1*$^{F/F}$*;Trp53*$^{F/F}$, WB1P; *WapCre;Brca1*$^{F/F}$*;Trp53*$^{F/F}$*;Col1a1*$^{invCAG\text{-}Myc/+}$, WB1P-Myc) breast cancer (Liu *et al*, 2007; Boelens *et al*, 2016; Annunziato *et al*, 2019). Unsupervised hierarchical clustering of gene expression profiles using a three-gene signature that distinguishes the PAM50 subtypes (Haibe-Kains *et al*, 2012) and principal component analysis (PCA) of global gene expression confirmed that tumors from WB1P-BE3 mice retained a basal-like transcriptional identity (Fig EV1B and C).

We then cloned a lentiviral vector encoding an sgRNA targeting the third exon of *Akt1* in order to establish an oncogenic E17K missense mutation by base editing (*Akt1*^{E17K}). To validate this sgRNA, we transduced NIH3T3 cells expressing an optimized BE3 enzyme, FNLS (Zafra *et al*, 2018), with Lenti-sg*Akt1*^{E17K} or a control Lenti-sgNT vector encoding a non-targeting sgRNA, and analyzed targeted editing at the *Akt1* locus by Sanger sequencing 5 days after transduction. Cells transduced with Lenti-sg*Akt1*^{E17K} showed extensive target C-to-T conversion, leading to oncogenic AKT1 E17K mutations (Fig 1A and B), as well as bystander edits at nearby cytosines with variable efficiency (Appendix Fig S2A). As off-target base editing activity of CBEs has recently been reported (Jin *et al*, 2019; Zuo *et al*, 2019), we performed whole-genome sequencing (WGS) of genomic DNA isolated from NIH3T3 cells with or without expression of the CBE and the sgRNAs, and performed genome-wide characterization of off-target single-nucleotide variants (SNVs). As expected, the on-target edits could be readily detected at high allele frequencies in CBE-expressing cells transduced with Lenti-sg*Akt1*^{E17K}. While a limited number of additional SNVs could be detected, none of these off-target edits generated missense or nonsense mutations or altered essential splice sites (Appendix Fig S3A).

To test the collaborative role of MYC overexpression and *Akt1*^{E17K} missense mutations *in vivo*, we generated lentiviral vectors encoding a *Myc*-overexpressing cassette together with the validated sg*Akt1*^{E17K} (Annunziato *et al*, 2019). These vectors (Lenti-sgNT-*Myc* and Lenti-sg*Akt1*^{E17K}-*Myc*) were injected intraductally into WB1P-BE3 females (Fig 1C). As expected, all mice from both groups developed mammary tumors in the injected glands with 100% penetrance (Fig 1D). WB1P-BE3 mice injected with Lenti-sgNT-*Myc* developed mammary tumors with a median latency of 72 days after injection ($n = 11$), closely resembling latencies previously observed for

 © 2020 The Authors

WB1P-Cas9 mice injected with the same construct (Annunziato *et al*, 2019). On the contrary, WB1P-BE3 mice injected with Lenti-sg*Akt1*^{E17K}-*Myc* developed tumors with a significantly shorter latency of 58 days (n = 12). Genomic DNA of mammary tumors from Lenti-sg*Akt1*^{E17K}-*Myc* injected WB1P-BE3 mice showed extensive editing of the target gene (Fig 1E and F), with greater than 78% average C-to-T conversion leading to activating *Akt1*^{E17K} missense mutations. Notably, bystander C-to-T editing and product purity at nearby cytosines of the protospacer were significantly lower, demonstrating positive selection specifically for oncogenic E17K mutations and not for other amino acid changes (Appendix Fig S2B and C). These results show that *in situ* base editing of the mammary

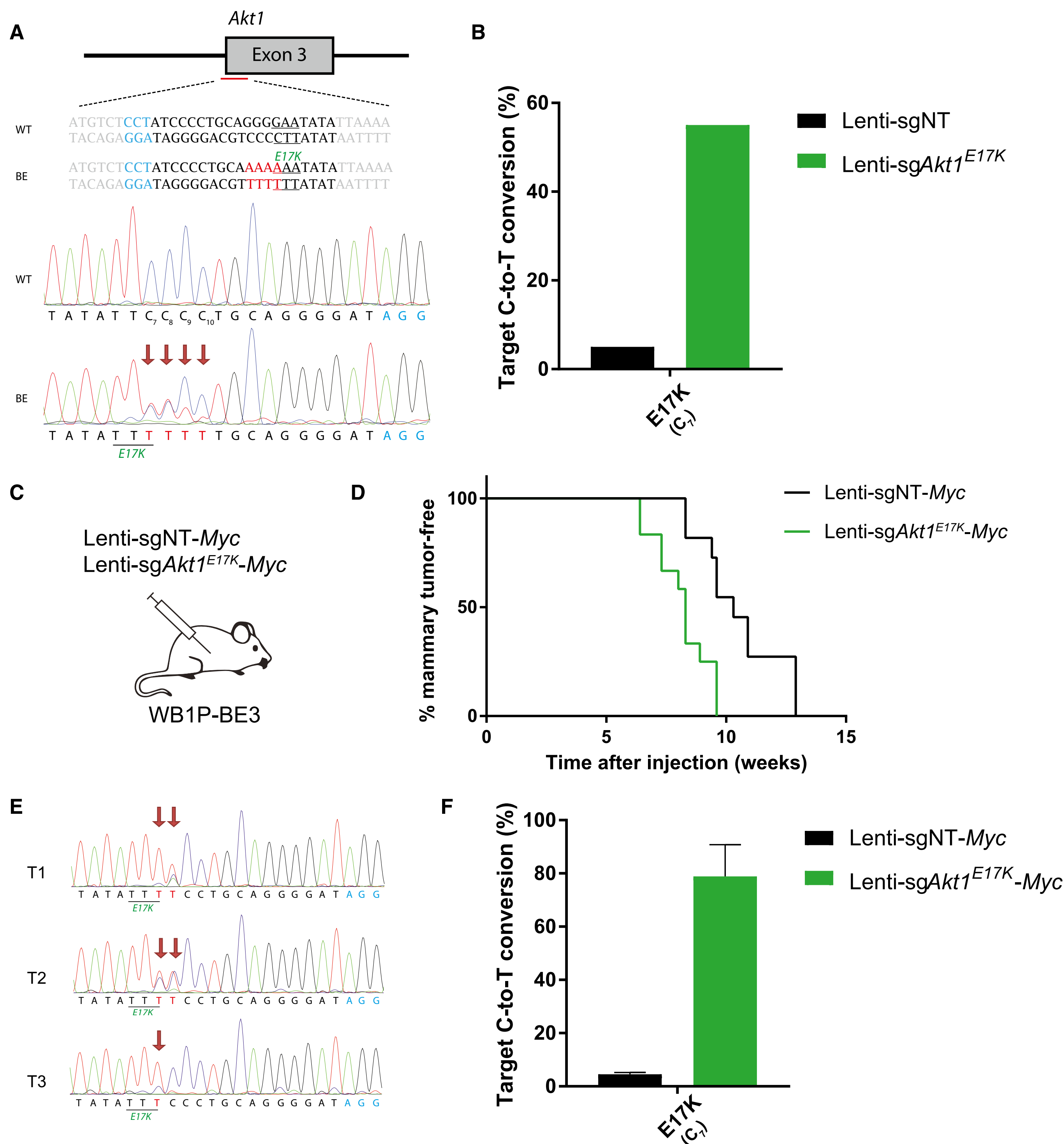

Figure 1.

Figure 1. *In vivo* installation of oncogenic mutations by base editing in a model of triple-negative breast cancer.

A Sanger-sequencing chromatograms showing the target region of sg*Akt1*^{E17K} in wild-type (WT) and base edited (BE) cells. Arrowheads highlight cytosines of the protospacer that show base editing 5 days after transduction of BE3-expressing NIH3T3 cells with Lenti-sg*Akt1*^{E17K}.

B EditR (Kluesner *et al*, 2018) was used to calculate the frequency (%) of C-to-T conversion at C_7 of the protospacer targeted by sg*Akt1*^{E17K} in BE3-expressing NIH3T3 cells 5 days after transduction with the indicated sgRNA vectors.

C Overview of the intraductal injections performed in *WapCre;Brca1*$^{F/F}$*;Trp53*$^{F/F}$*;Col1a1*$^{invCAG\text{-}BE3/+}$ (WB1P-BE3) females with high-titer lentiviruses encoding *Myc* cDNA and either a non-targeting (NT) sgRNA (Lenti-sgNT-*Myc*) or the sgRNA targeting *Akt1* (Lenti-sg*Akt1*^{E17K}-*Myc*).

D Kaplan–Meier curves showing mammary tumor-specific survival for the different models. WB1P-BE3 females injected with Lenti-sg*Akt1*^{E17K}-*Myc* (n = 12) showed a reduced mammary tumor-specific survival compared to WB1P-BE3 female mice injected with Lenti-sgNT-*Myc* (n = 11) vectors (58 days after injection vs. 72 days after injection, $P < 0.01$ by Mantel–Cox test).

E Sanger-sequencing chromatograms showing the target region of sg*Akt1*^{E17K} in three independent tumors from WB1P-BE3 females injected with Lenti-sg*Akt1*^{E17K}-*Myc*. Arrowheads highlight cytosines of the protospacer that show base editing.

F EditR was used to calculate the average frequency (%) of C-to-T conversion at C_7 of the protospacer in tumors from WB1P-BE3 females injected with Lenti-sgNT-*Myc* or Lenti-sg*Akt1*^{E17K}-*Myc*. Data are plotted as mean + standard deviation (n = 7).

gland enables modeling of defined point mutations within specific target genes.

We next tested whether this somatic platform could be used to generate an allelic series of missense mutations of an oncogene *in vivo*. The most frequent alterations observed in human BRCA1-associated TNBC, besides *TP53* alterations and *MYC* amplification, are *PIK3CA* missense variants (Annunziato *et al*, 2019; Jiang *et al*, 2019). We therefore designed multiple sgRNAs targeting *Pik3ca* and validated their ability to produce the hotspot E542K or E545K mutations (which are frequently observed in human tumors) or the much rarer E453K missense variant by base editing *in vitro* by Sanger sequencing and WGS (Fig 2A and B, Appendix Fig S3B). To test and compare the synergistic effect of MYC overexpression and *Pik3ca* missense mutations *in vivo*, we cloned Lenti-sg*Pik3ca-Myc* vectors encoding the specific sgRNAs targeting *Pik3ca*. The vectors were injected in WB1P-BE3 female mice (Fig 2C) and produced mammary tumors in all injected glands after variable latencies (Fig 2D). WB1P-BE3 females injected with Lenti-sg*Pik3ca*^{E542K}-*Myc* and Lenti-sg*Pik3ca*^{E545K}-*Myc* developed tumors significantly faster than Lenti-sgNT-*Myc* injected mice, with a median latency of 47 and 44 days after injection, respectively (n = 10 and n = 10). Notably, also mice injected with Lenti-sg*Pik3ca*^{E453K}-*Myc* developed tumors with a short median latency of 49 days (n = 10), underscoring that the *Pik3ca*^{E453K} mutation, albeit less frequent than *Pik3ca*^{E542K} and *Pik3ca*^{E545K} in human tumors, has similar cooperative effects in this setting. By target sequencing of the tumors, we found average C-to-T editing to be 69, 75, and 78% for *Pik3ca*^{E542K}, *Pik3ca*^{E545K}, and *Pik3ca*^{E453K}, respectively (Figs 2E and F, and EV2A). As an additional control, we designed an sgRNA targeting intron 9 of the *Pik3ca* gene (sg*Pik3ca*^{intron}), immediately downstream of the region targeted by sg*Pik3ca*^{E542K} and sg*Pik3ca*^{E545K}. As this region is reasonably distant from the exon–intron junction, we expected base conversions at this site to have neutral consequences on PIK3CA expression and activity. We validated the capability of sg*Pik3ca*^{intron} to produce specific C-to-T conversions at the target site *in vitro* by Sanger sequencing (Fig EV2B). We then cloned a Lenti-sg*Pik3ca*^{intron}-*Myc* construct which we injected intraductally into WB1P-BE3 mice. These mice developed tumors after a median latency of 67 days (n = 9), comparable to the tumor latency of WB1P-BE3 mice injected with Lenti-sgNT-*Myc* and significantly later than WB1P-BE3 mice injected with the codon-targeting Lenti-sg*Pik3ca-Myc* vectors (Fig EV2C). These data further support that the shortened tumor latency of the latter is due to the specific mutations installed by base editing.

The high C-to-T rates achieved *in vivo* with Lenti-sg*Akt1-Myc* and Lenti-sg*Pik3ca-Myc* vectors indicate that continuous editing during tumor progression could saturate base conversion at the target site in both copies of *Akt1* or *Pik3ca*. Therefore, we next tested whether we could apply *in situ* base editing for bi-allelic inactivation of a tumor suppressor gene. We designed an sgRNA targeting the tumor suppressor *Pten*, and we validated the capability of Lenti-sg*Pten*^{Q245*} to create nonsense editing *in vitro* by target sequencing and WGS (Fig 3A and B, Appendix Fig S3C). We then injected WB1P-BE3 mice with Lenti-sg*Pten*^{Q245*}-*Myc* vectors

Figure 2. *In situ* base editing creates allelic series of oncogenic driver mutations.

A Sanger-sequencing chromatograms showing the target regions of sg*Pik3ca*^{E542K}, sg*Pik3ca*^{E545K}, and sg*Pik3ca*^{E453K} in wild-type (WT) and base edited (BE) cells. Arrowheads highlight cytosines of the protospacers that show base editing 5 days after transduction of BE3-expressing NIH3T3 cells with Lenti-sg*Pik3ca*^{E542K}, Lenti-sg*Pik3ca*^{E545K}, and Lenti-sg*Pik3ca*^{E453K}.

B EditR was used to calculate the frequency (%) of C-to-T conversion at the indicated target cytosines of the protospacers in BE3-expressing NIH3T3 cells 5 days after transduction with the indicated sgRNA vectors.

C Overview of the intraductal injections performed in WB1P-BE3 females with high-titer lentiviruses encoding *Myc* and either a non-targeting sgRNA (Lenti-sgNT-*Myc*) or the different sgRNAs targeting *Pik3ca* (Lenti-sg*Pik3ca-Myc*).

D Kaplan–Meier curves showing mammary tumor-specific survival for the different models. WB1P-BE3 females injected with Lenti-sg*Pik3ca*^{E542K}-*Myc* (n = 10), Lenti-sg*Pik3ca*^{E545K}-*Myc* (n = 10), and Lenti-sg*Pik3ca*^{E453K}-*Myc* (n = 10) showed a reduced mammary tumor-specific survival compared to WB1P-BE3 female mice injected with Lenti-sgNT-*Myc* (n = 11) vectors (47, 44, and 49 days after injection, respectively vs. 72 days after injection, $P < 0.0001$ by Mantel–Cox test).

E Sanger-sequencing chromatograms showing the target region of sg*Pik3ca*^{E542K}, sg*Pik3ca*^{E545K}, and sg*Pik3ca*^{E453K} in three independent tumors from WB1P-BE3 females injected with the corresponding Lenti-sg*Pik3ca-Myc* vectors. Arrowheads highlight cytosines of the protospacer that show base editing.

F EditR was used to calculate the average frequency (%) of C-to-T conversion at the indicated target cytosines of the protospacers in tumors from WB1P-BE3 females injected with Lenti-sgNT-*Myc* or Lenti-sg*Pik3ca*^{E542K}-*Myc*, Lenti-sg*Pik3ca*^{E545K}-*Myc* and Lenti-sg*Pik3ca*^{E453K}-*Myc*. Data are plotted as mean + standard deviation (n = 7).

© 2020 The Authors

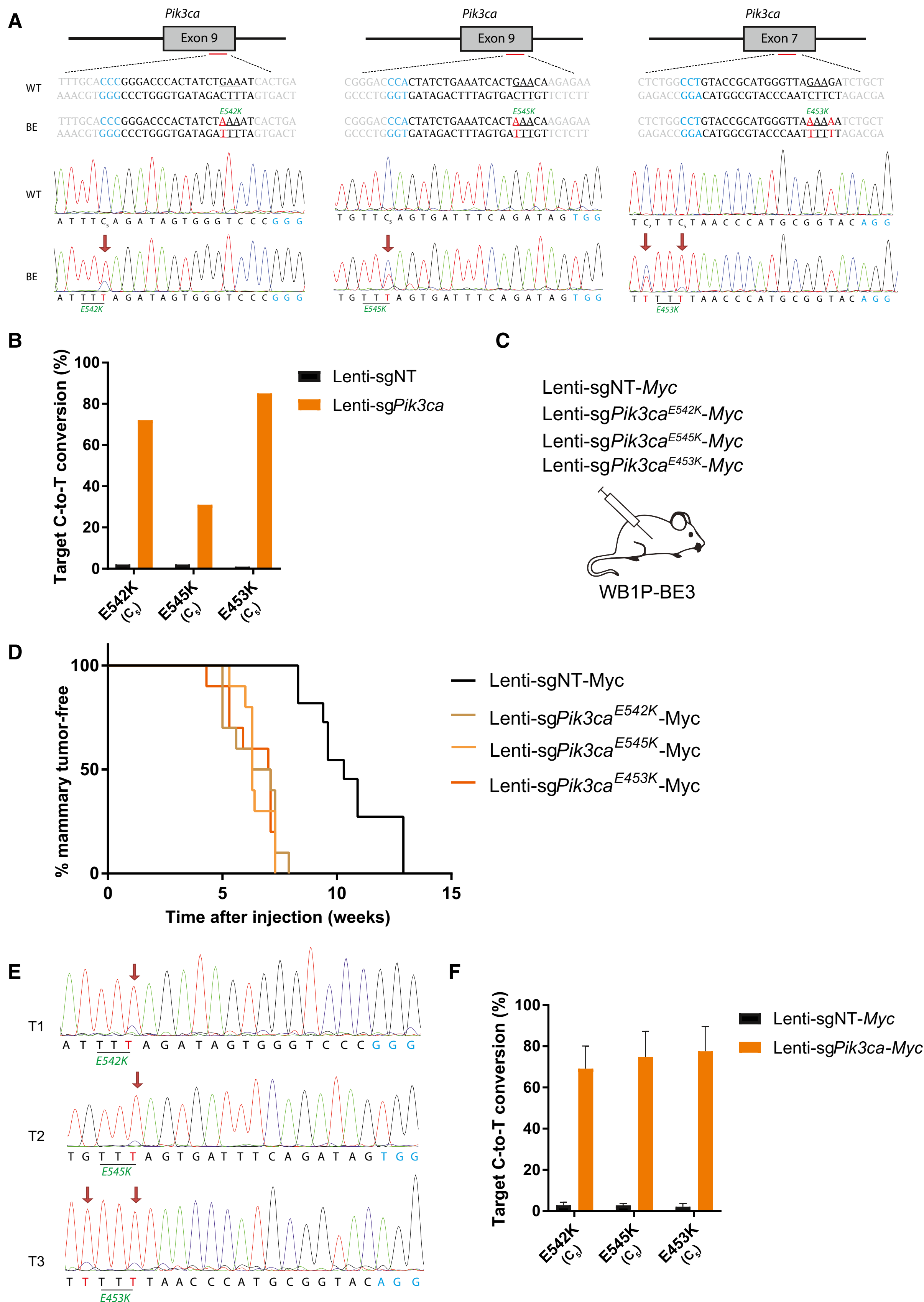

Figure 2.

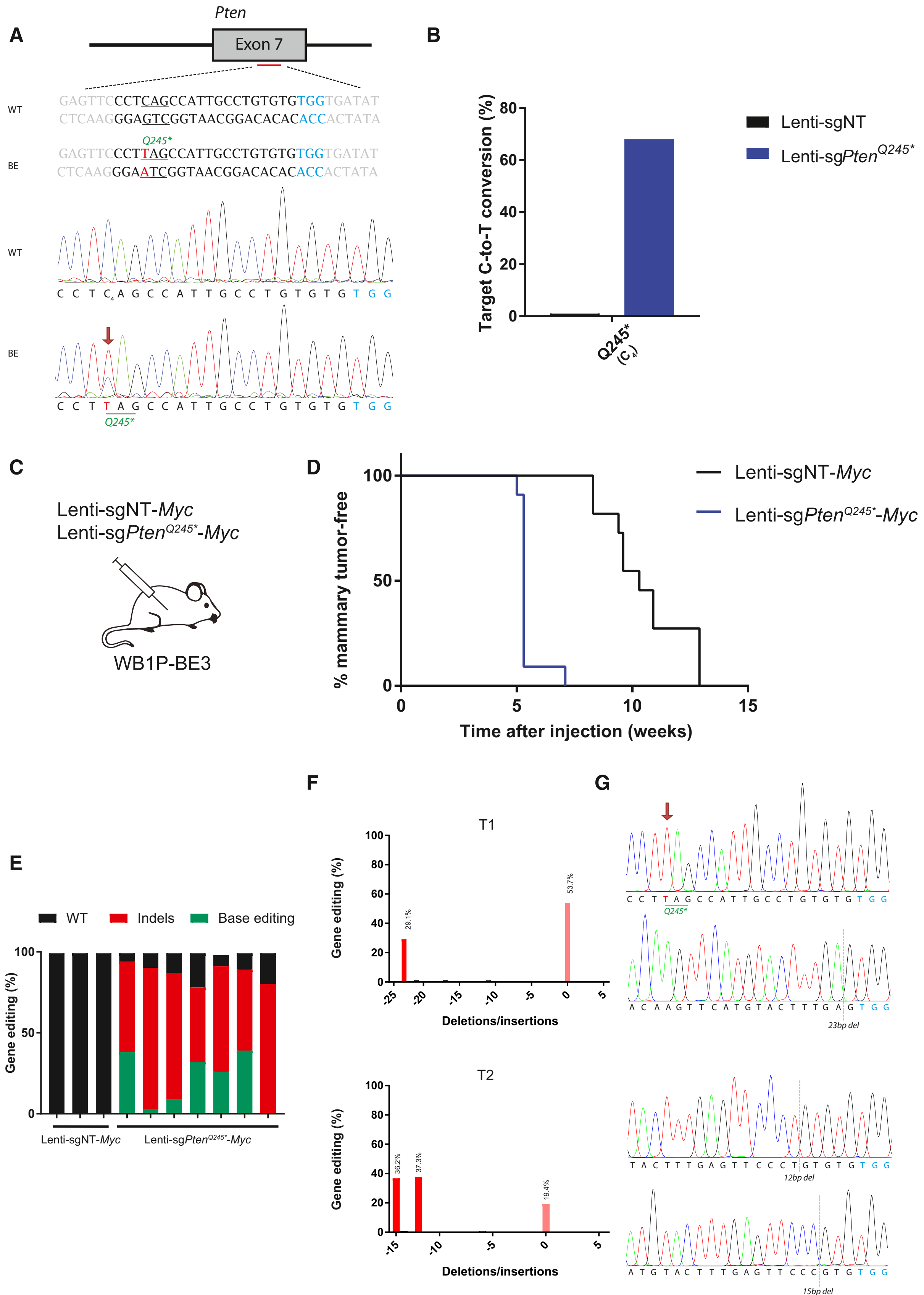

Figure 3.

© 2020 The Authors

Figure 3. *In vivo* nonsense editing of *Pten*.

A Sanger-sequencing chromatograms showing the target region of sg*Pten*^{Q245*} in wild-type (WT) and base edited (BE) cells. Arrowheads highlight cytosines of the protospacer that show base editing 5 days after transduction of BE3-expressing NIH3T3 cells with Lenti-sg*Pten*^{Q245*}.

B EditR was used to calculate the frequency (%) of C-to-T conversion at C_4 of the protospacer targeted by sg*Pten*^{Q245*} in BE3-expressing NIH3T3 cells 5 days after transduction with the indicated sgRNA vectors.

C Overview of the intraductal injections performed in WB1P-BE3 females with high-titer lentiviruses encoding *Myc* and either a non-targeting sgRNA (Lenti-sgNT-*Myc*) or the sgRNA targeting *Pten* (Lenti-sg*Pten*^{Q245*}-*Myc*).

D Kaplan–Meier curves showing mammary tumor-specific survival for the different models. WB1P-BE3 females injected with Lenti-sg*Pten*^{Q245*}-*Myc* (n = 11) showed a reduced mammary tumor-specific survival compared to WB1P-BE3 female mice injected with Lenti-sgNT-*Myc* (n = 11) vectors (37 days after injection vs. 72 days after injection, $P < 0.0001$ by Mantel–Cox test).

E BE Analyzer (Hwang *et al*, 2018) was used to assess from next-generation sequencing data the fraction of wild-type *Pten* alleles, base edited alleles, or alleles with insertions/deletions (indels) in tumors from WB1P-BE3 animals injected with Lenti-sgNT-*Myc* or Lenti-sg*Pten*^{Q245*}-*Myc*.

F TIDE analysis showing the spectrum of indels of the targeted *Pten* alleles in two independent representative tumors from WB1P-BE3 mice injected with Lenti-sg*Pten*^{Q245*}-*Myc*.

G For the two tumors shown in (F), Sanger-sequencing chromatograms showing the target region of sg*Pten*^{Q245*} (PCR products were subcloned for clarity). Arrowheads highlight cytosines of the protospacer that show base editing. In the lower example, the gene was inactivated by indels at both alleles, while in the upper one by Q245* base editing in one allele and a deletion at the second copy of the gene.

(n = 11) with the goal of overexpressing MYC and inactivating *Pten*, and observed accelerated TNBC formation in these mice compared with WB1P-BE3 mice injected with Lenti-sgNT-*Myc* (Fig 3C and D). The average latency (37 days after injection) was comparable to the mammary tumor-free survival of WB1P-Cas9 mice injected with the same Lenti-sg*Pten-Myc* construct (Annunziato *et al*, 2019), indicating that in both cases loss of function of *Pten* was collaborating with MYC overexpression in BRCA1-associated mammary tumorigenesis. On the contrary, WB1P mice injected with Lenti-sg*Pten*^{Q245*}-*Myc* (n = 11) developed TNBC with a median latency of 69 days, comparable to control tumors, further confirming that only the combined expression of BE3 and sg*Pten*^{Q245*} is responsible for the short tumor latency in WB1P-BE3 mice injected with Lenti-sg*Pten*^{Q245*}-*Myc* (Fig EV3A). Indeed, tumors from the latter group showed decreased PTEN levels and displayed activation of the PI3K/AKT downstream signaling pathway as visualized by immunoblot and immunohistochemical analysis of PTEN, phospho-Akt^{Ser473}, and phospho-S6$^{Ser235/236}$ expression (Figs EV3B and C, and EV4).

To characterize the phenotypes of the base edited mammary tumors described so far in more detail, we performed RNA sequencing on a panel of 29 additional tumors from WB1P-BE3 mice injected with different Lenti-sgRNA-*Myc* vectors, and compared their expression profiles to those of spontaneous WB1P-BE3 tumors. The tumors from the somatic models clustered together based on gene expression, but separated from spontaneous WB1P-BE3 tumors (Fig EV5A). Nonetheless, unsupervised hierarchical clustering of gene expression profiles using a three-gene signature that distinguishes the PAM50 subtypes (Haibe-Kains *et al*, 2012) and PCA analysis of global gene expression confirmed that all tumors from the somatic models retained a basal-like transcriptional identity (Fig EV5B and C). Histopathological analysis confirmed that they were all comparable to WB1P-BE3 tumors in terms of morphology and expression of ER, PR, HER2, E-cadherin, vimentin, keratin 8, and keratin 14, and despite higher MYC expression, they showed similar Ki-67 stainings (Figs EV4 and EV5D, Appendix Fig S4). Elevated phospho-S6$^{Ser235/236}$ expression was obvious only in tumors from WB1P-BE3 mice injected with Lenti-sg*Pten*^{Q245*}-*Myc*, and to a lower extent in tumors from WB1P-BE3 mice injected with Lenti-sg*Akt1*^{E17K}-*Myc*, but not in tumors from WB1P-BE3 mice injected with Lenti-sg*Pik3ca-Myc* vectors (Fig EV4). In accordance to this, gene set enrichment analysis (GSEA) indicated activation of the mTORC1 signaling in tumors from WB1P-BE3 mice injected with Lenti-sg*Pten*^{Q245*}-*Myc* and Lenti-sg*Akt1*^{E17K}-*Myc*, but not in tumors from WB1P-BE3 mice injected with Lenti-sg*Pik3ca-Myc* and Lenti-sgNT-*Myc* vectors (Appendix Fig S5).

Notably, target sequencing of *Pten* in tumors from WB1P-BE3 mice injected with Lenti-sg*Pten*^{Q245*}-*Myc* showed that in these specimens the gene was inactivated either by frame-shifting indels at both *Pten* alleles or by Q245* base edits in one allele and indels at the second copy of the gene (Fig 3E–G, Appendix Fig S6A). It was previously shown that BE3 can yield low but detectable unintended indels instead of base alterations *in vitro* (Komor *et al*, 2016). However, as we did not observe evident by-product indels in tumors somatically base edited with sg*Akt1* or sg*Pik3ca*, we reasoned that they might only become apparent in our somatic model when targeting a tumor suppressor gene like *Pten*, in which gene disruption by truncation is likely selected to the same extent as gene inactivation by nonsense mutation. To investigate this further, we designed and validated an sgRNA capable to install a Q97* ocher mutation in *Trp53 in vitro* by Sanger sequencing and WGS (Fig 4A and B, Appendix Fig S3D). Then, we generated *WapCre;Brca1*$^{F/F}$;*Trp53*$^{F/+}$;*Col1a1*$^{invCAG\text{-}BE3/+}$ mice with heterozygous *Trp53*^{F} floxed alleles and intraductally injected them with Lenti-sgNT-*Myc* or Lenti-sg*Trp53*^{Q97*}-*Myc* (Fig 4C). Moreover, to test the feasibility of multiplexed *in vivo* base editing, we also injected these mice with a tandem Lenti-sg*Pik3ca*^{E545K}/sg*Trp53*^{Q97*}-*Myc* vector that harbors two arrayed sgRNA cassettes, to simultaneously introduce the missense *Pik3ca*^{E545K} mutation and inactivate the residual wild-type copy of *Trp53*. *WapCre;Brca1*$^{F/F}$;*Trp53*$^{F/+}$;*Col1a1*$^{invCAG\text{-}BE3/+}$ females injected with Lenti-sgNT-*Myc* (n = 11) did not develop any palpable tumors during the 150 days of observation period (Fig 4D). In contrast, mice injected with Lenti-sg*Trp53*^{Q97*}-*Myc* and Lenti-sg*Pik3ca*^{E545K}/sg*Trp53*^{Q97*}-*Myc* developed TNBC tumors after a median latency of 101 and 76 days, respectively (n = 5 and n = 6). Most of the tumors from mice injected with Lenti-sg*Trp53*^{Q97*}-*Myc* and Lenti-sg*Pik3ca*^{E545K}/sg*Trp53*^{Q97*}-*Myc* displayed the targeted *Trp53*^{Q97*} mutation achieved by C-to-T base editing at C_8 of the protospacer (Fig 4E–G, Appendix Fig S6B), always together with a collateral edit at a nearby cytosine (C_6). Also in this case however, in some tumors the *Trp53* allele displayed a frame-shifting indel within the protospacer instead. Notably, target sequencing of *Trp53* showed that bystander editing at C_6 was still present in tumors with indels, suggesting that an initially base edited allele was re-targeted

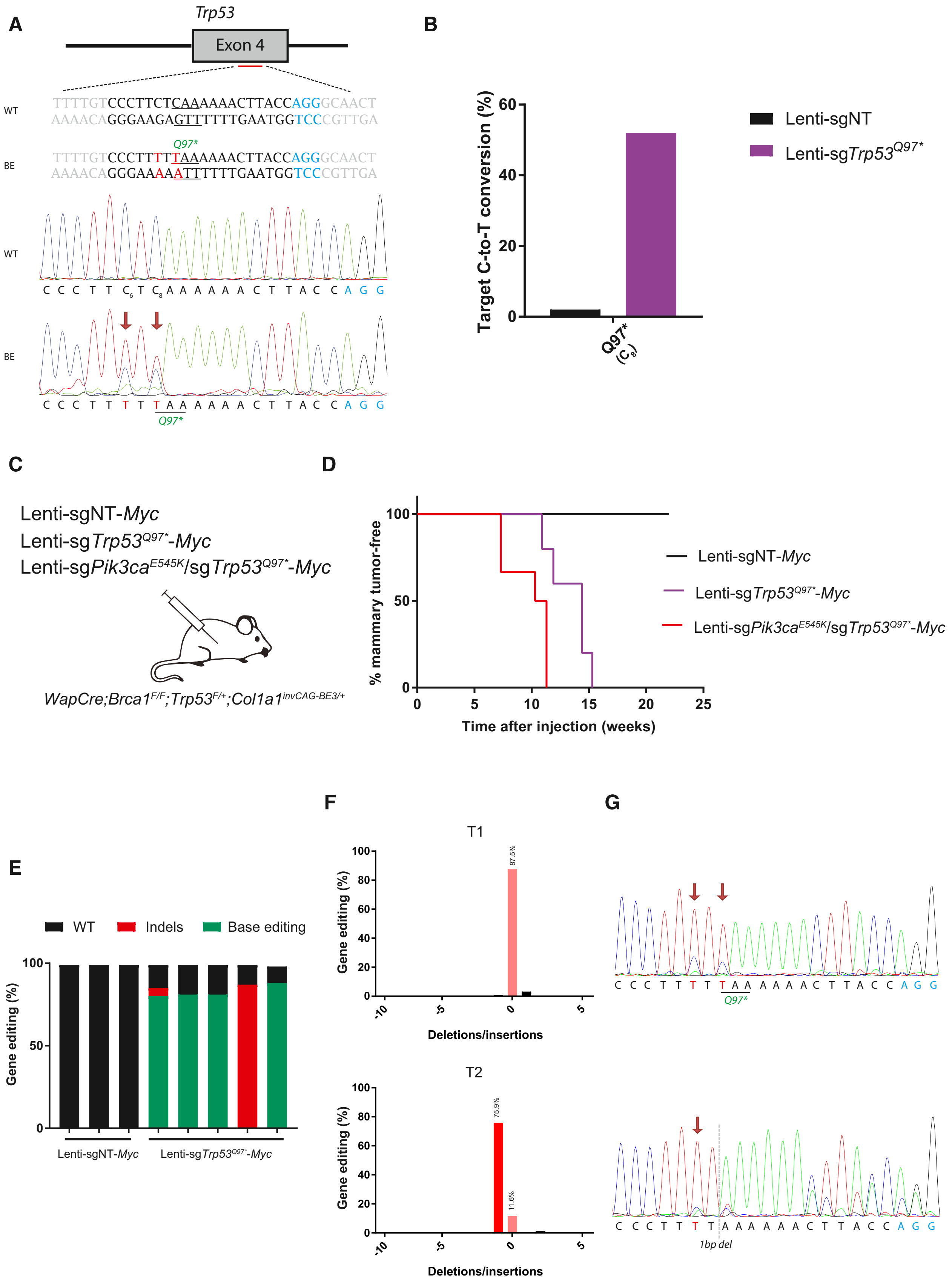

Figure 4.

 © 2020 The Authors

Figure 4. Multiplexed *in vivo* base editing.

A Sanger-sequencing chromatograms showing the target region of sg*Trp53*^{Q97*} in wild-type (WT) and base edited (BE) cells. Arrowheads highlight cytosines of the protospacer that show base editing 5 days after transduction of BE3-expressing NIH3T3 cells with Lenti-sg*Trp53*^{Q97*}.

B EditR was used to calculate the frequency (%) of C-to-T conversion at C_8 of the protospacer targeted by sg*Trp53*^{Q97*} in BE3-expressing NIH3T3 cells 5 days after transduction with the indicated sgRNA vectors.

C Overview of the intraductal injections performed in *WapCre;Brca1*$^{F/F}$;*Trp53*$^{F/+}$;*Col1a1*$^{invCAG\text{-}BE3/+}$ (*Trp53*^{F}-het WB1P-BE3) females with high-titer lentiviruses encoding *Myc* and either a non-targeting sgRNA (Lenti-sgNT-*Myc*), the sgRNA targeting *Trp53* (Lenti-sg*Trp53*^{Q97*}-*Myc*), or two arrayed sgRNA cassettes encoding sg*Pik3ca*^{E545K} and sg*Trp53*^{Q97*} (Lenti-sg*Pik3ca*^{E545K}/sg*Trp53*^{Q97*}-*Myc*).

D Kaplan–Meier curves showing mammary tumor-specific survival for the different models. *WapCre;Brca1*$^{F/F}$;*Trp53*$^{F/+}$;*Col1a1*$^{invCAG\text{-}BE3/+}$ females injected with Lenti-sg*Pik3ca*^{E545K}/sg*Trp53*^{Q97*}-*Myc* (n = 6) showed a reduced mammary tumor-specific survival compared to animals injected with Lenti-sg*Trp53*^{Q97*}-*Myc* (n = 5) vectors (76 days after injection vs. 101 days after injection, $P < 0.05$ by Mantel–Cox test). Females injected with Lenti-sgNT-*Myc* (n = 11) did not develop any palpable tumors during the 150 days of observation period.

E BE Analyzer was used to assess from next-generation sequencing data the fraction of wild-type *Trp53* alleles, base edited alleles, or alleles with indels in tumors from *WapCre;Brca1*$^{F/F}$;*Trp53*$^{F/+}$;*Col1a1*$^{invCAG\text{-}BE3/+}$ animals injected with Lenti-sg*Trp53*^{Q97*}-*Myc*. Tumors from WB1P-BE3 animals injected with Lenti-sgNT-*Myc* mice were used as control.

F TIDE analysis showing the spectrum of indels of the targeted *Trp53* alleles in two independent representative tumors from *WapCre;Brca1*$^{F/F}$;*Trp53*$^{F/+}$;*Col1a1*$^{invCAG\text{-}BE3/+}$ mice injected with Lenti-sg*Trp53*^{Q97*}-*Myc*.

G For the two tumors shown in (F), Sanger-sequencing chromatograms showing the target region of sg*Trp53*^{Q97*}. Arrowheads highlight cytosines of the protospacer that show base editing. In the lower example, the gene was inactivated by a deletion, while in the upper one by Q97* base editing. Of note, the allele with the indel also displays base editing at C_6 of the protospacer.

by the protracted activity of the CRISPR machinery, producing a DSB which was then resolved by indel-prone end-joining processes (Fig 4G). On the contrary, target sequencing of the *Pik3ca* gene confirmed that tumors induced by the tandem Lenti-sg*Pik3ca*^{E545K}/sg*Trp53*^{Q97*}-*Myc* vector displayed almost exclusively E545K base edits (79% average C-to-T editing), although bystander indels could be detected in a minor allele fraction upon deep sequencing (Appendix Fig S6C and D).

Discussion

Most human cancers are predominantly characterized by missense mutations. Here, we show that somatic base editing is feasible and effective at installing defined missense and nonsense mutations at endogenous loci in a mouse model of TNBC. The possibility to rapidly engineer breast cancer-associated point mutations *in situ* allows us to recapitulate gain-of-function mutations in known and putative oncogenes in preclinical models, and to evaluate the relative effect size of each genetic perturbation within an allelic series.

Somatic base conversion for cancer modeling has previously been achieved *in situ* by hydrodynamic injection of plasmids encoding BE3 and an sgRNA in the mouse tail vein, which led to oncogenic C-to-T editing at the β-catenin gene in the adult liver (Zafra *et al*, 2018). This approach is not applicable in the mammary gland, as we previously observed that *de novo* expression of Cas9 in adult mice elicits strong immune infiltration in this compartment, which could be circumvented by expressing the bacterial endonuclease from a conditional knock-in allele (Annunziato *et al*, 2016). Following the same paradigm, we report here the generation of a knock-in mouse model harboring a Cre-conditional BE3 allele, and its validation as a flexible and multiplexable platform for *in situ* base editing of the mammary gland upon intraductal delivery of sgRNA-encoding vectors. Using this system, we validated loss of function of *PTEN* and activation of *AKT1* and *PIK3CA* as *bona fide* drivers of BRCA1-associated tumorigenesis. Moreover, the possibility to rapidly derive cohorts of tumors engineered with defined mutations allowed us to evaluate the effect on tumorigenesis of different allelic variants of *Pik3ca*. This pipeline can also be used to test the effects of clinically relevant missense mutants on therapy response by orthotopic transplantation of tumor fragments or tumor-derived organoids into syngeneic mice (Rottenberg *et al*, 2010; Duarte *et al*, 2018).

A potential limitation of our system comes from the protracted expression of the CBE in the mammary gland of WB1P-BE3 mice, which often saturates base conversion at both alleles of an oncogene. This sustained expression could also increase off-target mutation rates and unintended by-product indel formation. Indeed, when targeting *Pten* and *Trp53* with the goal to install premature stop codons, we found a subset of the tumor suppressor alleles displayed gene inactivation by indels instead of nonsense edits. Possible solutions to minimize this downside could entail strategies to control editing dynamics using inducible or self-inactivating editors, selection against DSB formation with CBEs that encode DNA end-binding Gam proteins (Komor *et al*, 2017) or switch to systems based on nuclease-dead Cas9 rather than nickase. It is worth mentioning, however, that in cases where the effect of a missense mutation in a candidate cancer gene is unknown, the product promiscuity of our somatic platform could shed light on whether the functional consequence of the mutation is likely a gain of function or loss of function.

Two recent papers have shown that the CBE off-target mutation rate is higher than previously anticipated (Jin *et al*, 2019; Zuo *et al*, 2019). Although off-target activity of CBEs can be detrimental for therapeutic applications, it is much less of an issue for tumor acceleration studies in mouse models, in which random mutations collaborate with the genetically engineered mutations in driving tumorigenesis. This is particularly true in our TNBC mouse model, in which mammary tumorigenesis is induced by engineered loss of BRCA1 and p53, which results in loss of homologous recombination (HR) repair, genomic instability and a mutator phenotype. Still, while non-sequence-dependent off-targets can be experimentally controlled with neutral sgRNAs and biological replicates, sgRNA-dependent off-targets should be scrutinized on a case-by-case basis, preferentially by WGS.

Even with high-fidelity editors, a current limitation of CRISPR-mediated base editing is that not all missense variants can be modeled with the same enzymes. For example, the most prevalent *PIK3CA* mutation, H1047R, requires a G-to-A conversion that cannot

be produced with CBEs, but only with recently described adenine base editors (ABEs, Gaudelli *et al*, 2017). Moreover, to enable efficient base editing, a protospacer adjacent motif (PAM) needs to be present and appropriately distanced from a target base. Finally, some mutations that require C-to-non-T editing are less favored, especially with UGI-encoding editors. However, the base editing field is rapidly evolving to expand the range of targetable codons. Recently, base editors encoding alternative Cas9 orthologs or engineered SpCas9 variants that recognize a broader range of PAMs have been optimized (Hu *et al*, 2018; Nishimasu *et al*, 2018; Huang *et al*, 2019; Kleinstiver *et al*, 2019). In parallel, CBEs have been developed with reduced or expanded width of the editing window, to minimize bystander editing at non-target cytosines or to enlarge the repertoire of targetable bases, respectively (Kim *et al*, 2017; Jiang *et al*, 2018; Zafra *et al*, 2018; Tan *et al*, 2019; Thuronyi *et al*, 2019). Finally, base editors that efficiently convert target cytosines to a mixture of the other three bases have also been established (Hess *et al*, 2016) and might be particularly appealing for localized sequence diversification and mutagenesis *in vivo*. In general, as the catalog of base editors with specific properties continues to expand, it may be relevant to develop knock-in mice with conditional expression of additional base editing enzymes.

In conclusion, our *in vivo* base editor model offers novel opportunities for fast-track generation of somatic GEMMs of breast cancer. The conditional BE3 allele allows *in vivo* characterization of point mutations at a defined endogenous locus to assess their role in initiating or accelerating tumor formation in the mammary gland, alone or in combination with other conditional alleles. While we focused on TNBC in this study, the applicability of this strategy could be extended to other organs and tumor types by inter-crossing BE3 mice with different Cre-conditional mouse models.

Materials and Methods

sgRNA design

The sgRNAs for base editing were designed using Benchling (https://benchling.com). sg*Akt1*^{E17K}: TATATTCCCCTGCAGGGGAT; sg*Pik3ca*^{E545K}: TGTTCAGTGATTTCAGATAG; sg*Pik3ca*^{E542K}: ATTTCAGATAGTGGGTCCC; sg*Pik3ca*^{E453K}: TCTTCTAACCCATGCGGTAC; sg*Pik3ca*^{intron}: CTCTCAAGGCTGAAGGCCG; sg*Pten*^{Q245*}: CCTCAGCCATTGCCTGTGTG; sg*Trp53*^{Q97*}: CCCTTCTCAAAAAACTTACC.

Lentiviral vectors

The sgRNAs were cloned as described (Sanjana *et al*, 2014) into Lenti-U6-tdTomato-P2A-BlasR vectors (Lenti-sgRNA, Zafra *et al*, 2018, Addgene plasmid # 110854) or pGIN backbones (Evers *et al*, 2016). All vectors were validated by Sanger sequencing. The pGIN Lenti-sgNT-*Myc* vector, encoding *Myc* cDNA, and a non-targeting sgRNA (TGATTGGGGGTCGTTCGCCA) were described before (Annunziato *et al*, 2019). For cloning of other Lenti-sgRNA-*Myc* vectors, XbaI and XhoI were used to extract a *Myc*-encoding fragment from Lenti-sgNT-*Myc*, which was inserted in the XbaI-XhoI digested backbones of the pGIN vectors encoding the different sgRNAs. For cloning of the Lenti-sg*Pik3ca*^{E545K}/sg*Trp53*^{Q97*}-*Myc* tandem vector, a fragment encoding sg*Pik3ca*^{E545K} was amplified by PCR from Lenti-sg*Pik3ca*^{E545K}-*Myc* using XbaI-containing primers and cloned in the XbaI digested backbone of Lenti-sg*Trp53*^{Q97*}-*Myc*. pLenti-FNLS-P2A-Puro was a gift from Lukas Dow (Zafra *et al*, 2018, Addgene plasmid # 110841). Concentrated stocks of VSV-G pseudotyped lentivirus were produced by transient co-transfection of four plasmids in 293T as previously described (Follenzi *et al*, 2000). Lentiviral titers were determined using the qPCR lentivirus titration kit from Abm (LV900).

Cell culture

293T cells for lentiviral production and NIH3T3 cells were cultured in Iscove's medium (Invitrogen Life Technologies) containing 10% FBS, 100 IU ml^{-1} penicillin, and 100 μg ml^{-1} streptomycin. All transductions were performed by adding diluted viral supernatant to the cells in the presence of 8 μg ml^{-1} polybrene (Sigma). For testing of sgRNA activity *in vitro*, NIH3T3 cells were first transduced with pLenti-FNLS-P2A-Puro, and after 3 days of 2 μg ml^{-1} puromycin selection, they were re-transduced with the different Lenti-sgRNA vectors and selected for 4 days with 4 μg ml^{-1} blasticidin. Harvesting of cells for genomic DNA isolation was performed 5 days after transduction with the Lenti-sgRNA vectors.

PCRs, Sanger sequencing, and EditR analyses

Genomic DNA from frozen cell pellets was isolated using the Gentra Puregene genomic DNA isolation kit from Qiagen. For Sanger sequencing, amplification of base edited targets was performed with specific primers spanning the target sites (FW_Akt1: CCTGCGTATGGCTGATGTTG; RV_Akt1: CCCGCATGGCTAAGACACTT; FW_Pik3ca_1: AGTGGAGTGTAGGAAGAGCCT; RV_Pik3ca_1: ACAGGAAGAAGGTCCCTCGG; FW_Pik3ca_2: ACCCTAGTGTCCGGGAAAATG; RV_Pik3ca_2: AGAGCTCAACAGTAGCCACAC; FW_Pten: TGTATTTAACCACACAGATCCTCA; RV_Pten: AACAAACTAAGGGTCGGGGC; FW_Trp53: CTTTGGTGTTGGGCTGGTAG; RV_Trp53: GGGCAAAACTAAACTCTGAGGC) and 1 μg DNA template using the Q5 high-fidelity PCR kit from NEB. Amplicons were sequenced using the FW primer, and CRISPR/Cas9-induced base edits were quantified as described with EditR (Kluesner *et al*, 2018, https://moriaritylab.shinyapps.io/editr_v10). Untransduced cells were taken along as a control in each amplification.

Mouse studies

pCMV-BE3 was a gift from David Liu (Addgene plasmid # 73021). BE3 cDNA was sequence-verified and inserted as FseI-NotI fragments into the *Frt-invCag-IRES-Luc* shuttle vector (Huijbers *et al*, 2014), resulting in *Frt-invCag-BE3*. Flp-mediated knock-in of the shuttle vector in the *WapCre;Brca1*$^{F/F}$*;Trp53*$^{F/F}$*;Col1a1-frt* GEMM-ESC was performed as described (Huijbers *et al*, 2014). Chimeric animals were crossed with *Brca1*$^{F/F}$*;Trp53*$^{F/F}$ mice to generate the experimental cohorts. *WapCre*, *Brca1*$^{F/F}$, *Trp53*$^{F/F}$, and knock-in alleles were detected using PCR as described (Derksen *et al*, 2006; Liu *et al*, 2007; Huijbers *et al*, 2014). Intraductal injections were performed as described (Krause *et al*, 2013; Annunziato *et al*, 2016). Lentiviral titers ranging from 2 to 20×10^8 TU ml^{-1} were used. Animal experiments were approved by the Animal Ethics Committees of the Netherlands Cancer Institute. Mice were bred and

 © 2020 The Authors

maintained in accordance with institutional, national and European guidelines for Animal Care and Use.

Statistical analysis

Log-rank Mantel–Cox test was used for the following figures: Figs 1D, 2D, 3D, 4D, EV2C, and EV3A.

Immunoblotting

Protein lysates were made using lysis buffer (20 mM Tris pH 8.0, 300 mM NaCl, 2% NP-40, 20% glycerol, 10 mM EDTA) complemented with protease inhibitors (Roche) and quantified using the BCA Protein Assay Kit (Pierce). Protein lysates were loaded onto a 4–12% Bis-Tris gradient gel (Invitrogen) and transferred on a nitrocellulose membrane (Bio-Rad) in transfer buffer (38 mM glycine, 5 mM TRIS, and 0.01% SDS in PBS-T (0.5% Tween-20)). Membranes were blocked in 5% w/v bovine serum albumin (BSA) in PBS-T after which they were stained for 2 h at room temperature using the primary antibodies anti-AKT1 [1:1,000, Cell Signaling Technology (CST) 2938], anti-phospho-AKT1^{Ser473} (1:2,000, CST 4060), anti-p44/42 MAPK (1:1,000, CST 4695), anti-phospho-p44/42 MAPK ERK1/ERK2$^{Thr202/Tyr204}$ (1:2,000 CST 9101), anti-S6 (1:1,000, CST 2217), anti-phospho-S6$^{Ser235/Ser236}$ (1:2,000, CST 2211), anti-PTEN (1:1,000 CST 9188), and anti-β-actin (1:50,000, Sigma A5441) in 5% w/v BSA in PBS-T. Membranes were washed three times with 1% BSA in PBS-T and incubated for 1 h with an HRP-conjugated secondary antibody (1:2,000, DAKO). Stained membranes were washed three times in 1% BSA in PBS-T and developed using Pierce ECL Western Blotting Substrate (Thermo Scientific).

Histology and immunohistochemistry

Tissues were formalin-fixed overnight and paraffin-embedded by routine procedures. Hematoxylin and eosin staining was performed as described (Doornebal *et al*, 2013). Immunohistochemical stainings were processed as described (Doornebal *et al*, 2013; Henneman *et al*, 2015). For ER, PR, and phospho-S6$^{Ser235/Ser236}$, primary mouse antibody anti-ER (Santa Cruz sc-542), anti-PR (Thermo Scientific RM-9102), and anti-phospho-S6$^{Ser235/Ser236}$ (CST 2211) were used. For HER2, E-cadherin, vimentin, keratin 14, Myc and Ki-67, primary rabbit antibody anti-NEU (Santa Cruz sc-284), anti E-cadherin (CST 3195), anti-vimentin (CST 5741), anti-cytokeratin 14 (Abcam ab181595), anti-MYC (Abcam ab32072), and anti-Ki-67 (Abcam ab15580) were used. For keratin 8, primary rat antibody anti-cytokeratin 8 (University of Iowa TROMA-1) was used. All slides were digitally processed using the Aperio ScanScope (Aperio, Vista, CA, USA) and captured using ImageScope software version 12.0.0 (Aperio).

Deep target sequencing of tumor fragments

Frozen tumor pieces were lysed overnight in lysis buffer (100 mM Tris–HCl, 5 mM EDTA, 0.2% SDS, 200 mM NaCl, and 100 μg ml^{-1} Proteinase-K), and genomic DNA was purified with standard phenol–chloroform extraction. For deep sequencing, amplification of base edited targets was performed with specific primers spanning the target sites and including the Phased PE adapter sequence (FW_PE-Pten: ACACTCTTTCCCTACACGACGCTCTTCCGATCTTGTGGTCTGCCAGCTAAAGG; RV_PE-Pten: CGGTCTCGGCATTCCTGCTGAACCGCTCTTCCGATCTCCACAGAAATGAAGAGTCTGCC; FW_PE-Trp53: ACACTCTTTCCCTACACGACGCTCTTCCGATCTTTTTGAAGGCCCAAGTGAAGC; RV_PE-Trp53: CGGTCTCGGCATTCCTGCTGAACCGCTCTTCCGATCTAGGCATTGAAAGGTCACACGA; FW_PE-Pik3ca: ACACTCTTTCCCTACACGACGCTCTTCCGATCTAGCACCAGTTTGCTTTTTCAAAT; RV_PE-Pik3ca: CGGTCTCGGCATTCCTGCTGAACCGCTCTTCCGATCTGACAGGAAGAAGGTCCCTCG) using Platinum Taq DNA Polymerase High Fidelity (ThermoFisher). Indexed libraries were sequenced using Illumina MiSeq technologies (Paired End 250 bp runs spiked with 50% PhiX). CRISPR/Cas9-induced base edits and indels were quantified as described with BE Analyzer (Hwang *et al*, 2018, http://www.rgenome.net/be-analyzer). For Sanger sequencing, amplification of base edited targets was performed similarly as for cells. Amplicons were sequenced using the FW primer and CRISPR/Cas9-induced base edits and indels were quantified as described with EditR and TIDE (Kluesner *et al*, 2018, https://moriaritylab.shinyapps.io/editr_v10; Brinkman *et al*, 2014, http://tide.nki.nl). Untransduced cells were taken along as a control in each amplification.

Generation and analysis of RNA sequencing data

The mRNA library was generated using Illumina TruSeq Stranded mRNA Library Prep Kit and sequenced with 65 base single reads on HiSeq 2500. The sequencing reads were first trimmed using Cutadapt (v.1.13) to remove any residual adapter sequences and filter the short reads smaller than 20 bp after trimming the adapter sequences. The trimmed reads were then mapped to the reference genome (Ensembl GRCm38) using STAR aligner (v.2.5.2b; Dobin *et al*, 2013). The aligned reads were quantified using featureCounts (v. 1.5.2; Liao *et al*, 2014) based on the gene annotation from Ensembl GRCm38 version 89. The raw gene read counts were normalized by TMM normalization using edgeR (Robinson *et al*, 2010), and count per million (CPM) values were computed using limma-voom (Law *et al*, 2014). Genes with CPM < 1 across the entire samples were excluded for downstream analysis to reduce the false positives that can derive from lowly expressed genes.

The RNA sequencing data for basal (KB1P, WB1P, and WB1P-Myc) and luminal (WEP) tumors were obtained from previous studies from our group (Annunziato *et al*, 2019). For integration with our new dataset, we used the raw read counts that were derived from the same pipeline. The raw read counts for the new and previous datasets were then normalized together using TMM normalization, and CPM values were computed using edgeR and limma-voom, as described above. Genes with CPM < 1 across the entire samples were excluded for downstream analysis. Gene set enrichment analysis was performed using fgsea with the gene set "MTORC1_SIGNALING" in the MSigDB Hallmark gene set collection (Liberzon *et al*, 2015). Moderated *t*-statistics from limma-voom (Law *et al*, 2014) was used to rank the genes, and the permutation for each gene set was conducted 10,000 times to obtain an empirical null distribution.

Generation and analysis of whole-genome sequencing data

Whole-genome sequencing libraries were prepared using standard protocols for the Illumina X10 platform. The resulting sequence was aligned using bwa-mem (v.0.7.17) to the reference mouse GRCm38

© 2020 The Authors

assembly, and PCR duplicates were marked using bamstreamingmarkduplicates in biobambam (v.2.0.79). The total mapped coverage varied from 24× to 44×, with a median of 37×. To identify off-target edits in cell lines with a targeting sgRNA, variant calling was performed using cgpCaVEManWrapper (v1.13.14; Jones *et al*, 2016) and cgpPindel (v3.3.0 Raine *et al*, 2015), using a control (with no sgRNA) as the reference sample. The raw CaVEMan and Pindel calls were merged, and the bcftools (Li, 2011) SnpGap filter was used to remove SNVs that were within 15 bp of an indel, as these are likely false-positive variants that are a result of mismatches from read alignment issues. Further false-positive variants were further filtered by selecting the "pass" calls tagged from the cgpCaVEMan and cgpPindel default filtering, excluding calls (unfiltered) found in a second control (cells transduced with a non-targeting sgRNA), indels in simple repeats, and variants in common laboratory mouse strains from the Mouse Genomes Project (release version 6; Doran *et al*, 2016). To remove additional false-positive calls, indel calls that fell inside of any type of repeat were excluded, unless the whole repeat was deleted. Indel calls with at least 1 alternate allele in the reference sample (no sgRNA) were excluded. The following cgpCaVEMan filters were applied to SNVs: CLPM = 0 (no soft-clipped bases in the reads with the variant) and ASMD ≥ 130 (median alignment score of the reads with the variant). Variant calls with either allele frequency (AF) < 0.1, less than 5 variant-supporting reads (minimum base quality score 30), or at least 1 alternative allele in either control samples (minimum base quality score 30) were also considered false positives. SNV and indel calls at sites with less than 10× total coverage in either the reference or query samples were also excluded. After visual inspection of the read alignments for remaining indel calls and comparison to the same regions in the controls, it was determined that these calls were likely false-positive indels. To determine which SNVs are potentially deleterious, VAGrENT (Menzies *et al*, 2015) was used to identify missense mutations, nonsense mutations, and variants altering essential splice sites.

Data availability

The RNA-Seq data produced in this study are available in the following database: ENA Accession PRJEB34212 (http://www.ebi.ac.uk/ena/data/view/PRJEB34212). The WGS data produced in this study are available in the following database: ENA Accession ERP116589 (http://www.ebi.ac.uk/ena/data/view/ERP116589).

Expanded View for this article is available online.

Acknowledgements
We thank Koen Schipper, Sjoerd Klarenbeek, Elizabeth Anderson, and Antoinette van Weverwijk for technical suggestions, and/or help with the experiments. We are grateful for excellent support from the NKI animal facility, animal pathology facility, transgenic facility, preclinical intervention unit, core facility molecular pathology and biobanking (CFMPB), and genomics core facility. Financial support was provided by the Oncode Institute, the Netherlands Organization for Scientific Research (NWO: Cancer Genomics Netherlands (CGCNL; grant 024001028), Cancer Systems Biology Center (CSBC; grant 85300120), Netherlands Genomics Initiative (NGI) Zenith grant 93512009, VICI grant 91814643), the European Research Council (ERC Synergy project CombatCancer, grant 319661), and a NWO National Roadmap grant for Large-Scale Research Facilities (grant 184032303).

Author contributions
Conceptualization: SA, CL, and JJ. Experiments: SA, CL, LH, JB, KW, BS, BvG, RdK-G, APD, EvdB, TE, SM, and KB. Supervision: LFAW, DJA, MvdV, IJH, LED, and JJ. Resources: MPZ, EMS, and LED. Data analysis: SA, CL, and JJ. Writing: SA, CL, and JJ with support from DJA and LED.

Conflict of interest
The authors declare that they have no conflict of interest.

References

Annunziato S, Kas SM, Nethe M, Yücel H, Del Bravo J, Pritchard C, Bin Ali R, van Gerwen B, Siteur B, Drenth AP *et al* (2016) Modeling invasive lobular breast carcinoma by CRISPR/Cas9-mediated somatic genome editing of the mammary gland. *Genes Dev* 30: 1470 – 1480

Annunziato S, de Ruiter JR, Henneman L, Brambillasca CS, Lutz C, Vaillant F, Ferrante F, Drenth AP, van der Burg E, Siteur B *et al* (2019) Comparative oncogenomics identifies combinations of driver genes and drug targets in BRCA1-mutated breast cancer. *Nat Commun* 10: 397

Boelens MC, Nethe M, Klarenbeek S, de Ruiter JR, Schut E, Bonzanni N, Zeeman AL, Wientjens E, van der Burg E, Wessels L *et al* (2016) PTEN loss in E-cadherin-deficient mouse mammary epithelial cells rescues apoptosis and results in development of classical invasive lobular carcinoma. *Cell Rep* 16: 2087 – 2101

Brinkman EK, Chen T, Amendola M, van Steensel B (2014) Easy quantitative assessment of genome editing by sequence trace decomposition. *Nucleic Acids Res* 42: e168

Derksen PW, Liu X, Saridin F, van der Gulden H, Zevenhoven J, Evers B, van Beijnum JR, Griffioen AW, Vink J, Krimpenfort P *et al* (2006) Somatic inactivation of E-cadherin and p53 in mice leads to metastatic lobular mammary carcinoma through induction of anoikis resistance and angiogenesis. *Cancer Cell* 10: 437 – 449

Dobin A, Davis CA, Schlesinger F, Drenkow J, Zaleski C, Jha S, Batut P, Chaisson M, Gingeras TR (2013) STAR: ultrafast universal RNA-seq aligner. *Bioinformatics* 29: 15 – 21

Doornebal CW, Klarenbeek S, Braumuller TM, Klijn CN, Ciampricotti M, Hau CS, Hollmann MW, Jonkers J, de Visser KE (2013) A preclinical mouse model of invasive lobular breast cancer metastasis. *Cancer Res* 73: 353 – 363

Doran AG, Wong K, Flint J, Adams DJ, Hunter KW, Keane TM (2016) Deep genome sequencing and variation analysis of 13 inbred mouse strains defines candidate phenotypic alleles, private variation and homozygous truncating mutations. *Genome Biol* 17: 167

Duarte AA, Gogola E, Sachs N, Barazas M, Annunziato S, R de Ruiter J, Velds A, Blatter S, Houthuijzen JM, van de Ven M *et al* (2018) BRCA-deficient mouse mammary tumor organoids to study cancer-drug resistance. *Nat Methods* 15: 134 – 140

Evers B, Jastrzebski K, Heijmans JP, Grernrum W, Beijersbergen RL, Bernards R (2016) CRISPR knockout screening outperforms shRNA and CRISPRi in identifying essential genes. *Nat Biotechnol* 34: 631 – 633

Follenzi A, Ailles LE, Bakovic S, Geuna M, Naldini L (2000) Gene transfer by lentiviral vectors is limited by nuclear translocation and rescued by HIV-1 pol sequences. *Nat Genet* 25: 217 – 222

Gaudelli NM, Komor AC, Rees HA, Packer MS, Badran AH, Bryson DI, Liu DR (2017) Programmable base editing of A•T to G•C in genomic DNA without DNA cleavage. *Nature* 551: 464 – 471

 © 2020 The Authors

Haibe-Kains B, Desmedt C, Loi S, Culhane AC, Bontempi G, Quackenbush J, Sotiriou C (2012) A three-gene model to robustly identify breast cancer molecular subtypes. *J Natl Cancer Inst* 104: 311 – 325

Henneman L, van Miltenburg MH, Michalak EM, Braumuller TM, Jaspers JE, Drenth AP, de Korte-Grimmerink R, Gogola E, Szuhai K, Schlicker A *et al* (2015) Selective resistance to the PARP inhibitor olaparib in a mouse model for BRCA1-deficient metaplastic breast cancer. *Proc Natl Acad Sci USA* 112: 8409 – 8414

Hess GT, Frésard L, Han K, Lee CH, Li A, Cimprich KA, Montgomery SB, Bassik MC (2016) Directed evolution using dCas9-targeted somatic hypermutation in mammalian cells. *Nat Methods* 13: 1036 – 1042

Hu JH, Miller SM, Geurts MH, Tang W, Chen L, Sun N, Zeina CM, Gao X, Rees HA, Lin Z *et al* (2018) Evolved Cas9 variants with broad PAM compatibility and high DNA specificity. *Nature* 556: 57 – 63

Huang TP, Zhao KT, Miller SM, Gaudelli NM, Oakes BL, Fellmann C, Savage DF, Liu DR (2019) Circularly permuted and PAM-modified Cas9 variants broaden the targeting scope of base editors. *Nat Biotechnol* 37: 626 – 631

Huijbers IJ, Bin Ali R, Pritchard C, Cozijnsen M, Kwon MC, Proost N, Song JY, de Vries H, Badhai J, Sutherland K *et al* (2014) Rapid target gene validation in complex cancer mouse models using re-derived embryonic stem cells. *EMBO Mol Med* 6: 212 – 225

Hwang GH, Park J, Lim K, Kim S, Yu J, Yu E, Kim ST, Eils R, Kim JS, Bae S (2018) Web-based design and analysis tools for CRISPR base editing. *BMC Bioinformatics* 19: 542

Jiang W, Feng S, Huang S, Yu W, Li G, Yang G, Liu Y, Zhang Y, Zhang L, Hou Y *et al* (2018) BE-PLUS: a new base editing tool with broadened editing window and enhanced fidelity. *Cell Res* 28: 855 – 861

Jiang YZ, Ma D, Suo C, Shi J, Xue M, Hu X, Xiao Y, Yu KD, Liu YR, Yu Y *et al* (2019) Genomic and transcriptomic landscape of triple-negative breast cancers: subtypes and treatment strategies. *Cancer Cell* 35: 428 – 440.e5

Jin S, Zong Y, Gao Q, Zhu Z, Wang Y, Qin P, Liang C, Wang D, Qiu JL, Zhang F *et al* (2019) Cytosine, but not adenine, base editors induce genome-wide off-target mutations in rice. *Science* 364: 292 – 295

Jones D, Raine KM, Davies H, Tarpey PS, Butler AP, Teague JW, Nik-Zainal S, Campbell PJ (2016) cgpCaVEManWrapper: simple execution of CaVEMan in order to detect somatic single nucleotide variants in NGS data. *Curr Protoc Bioinformatics* 56: 15.10.1 – 15.10.18

Kas SM, de Ruiter JR, Schipper K, Annunziato S, Schut E, Klarenbeek S, Drenth AP, van der Burg E, Klijn C, Ten Hoeve JJ *et al* (2017) Insertional mutagenesis identifies drivers of a novel oncogenic pathway in invasive lobular breast carcinoma. *Nat Genet* 49: 1219 – 1230

Kim YB, Komor AC, Levy JM, Packer MS, Zhao KT, Liu DR (2017) Increasing the genome-targeting scope and precision of base editing with engineered Cas9-cytidine deaminase fusions. *Nat Biotechnol* 35: 371 – 376

Kleinstiver BP, Sousa AA, Walton RT, Tak YE, Hsu JY, Clement K, Welch MM, Horng JE, Malagon-Lopez J, Scarfò I *et al* (2019) Engineered CRISPR-Cas12a variants with increased activities and improved targeting ranges for gene, epigenetic and base editing. *Nat Biotechnol* 37: 276 – 282

Kluesner MG, Nedveck DA, Lahr WS, Garbe J, Abrahante J, Webber B, Moriarty BS (2018) EditR: A method to quantify base editing via Sanger sequencing. *CRISPR J* 1: 239 – 250

Komor AC, Kim YB, Packer MS, Zuris JA, Liu DR (2016) Programmable editing of a target base in genomic DNA without double-stranded DNA cleavage. *Nature* 533: 420 – 424

Komor AC, Zhao KT, Packer MS, Gaudelli NM, Waterbury AL, Koblan LW, Kim YB, Badran AH, Liu DR (2017) Improved base excision repair inhibition and bacteriophage Mu Gam protein yields C:G-to-T: a base editors with higher efficiency and product purity. *Sci Adv* 3: eaao4774

Krause S, Brock A, Ingber DE (2013) Intraductal injection for localized drug delivery to the mouse mammary gland. *J Vis Exp* 80: 50692

Law CW, Chen Y, Shi W, Smyth GK (2014) voom: Precision weights unlock linear model analysis tools for RNA-seq read counts. *Genome Biol* 15: R29

Li H (2011) A statistical framework for SNP calling, mutation discovery, association mapping and population genetical parameter estimation from sequencing data. *Bioinformatics* 27: 2987 – 2993

Liao Y, Smyth GK, Shi W (2014) featureCounts: an efficient general purpose program for assigning sequence reads to genomic features. *Bioinformatics* 30: 923 – 930

Liberzon A, Birger C, Thorvaldsdóttir H, Ghandi M, Mesirov JP, Tamayo P (2015) The Molecular Signatures Database (MSigDB) hallmark gene set collection. *Cell Syst* 1: 417 – 425

Liu X, Holstege H, van der Gulden H, Treur-Mulder M, Zevenhoven J, Velds A, Kerkhoven RM, van Vliet MH, Wessels LF, Peterse JL *et al* (2007) Somatic loss of BRCA1 and p53 in mice induces mammary tumors with features of human BRCA1-mutated basal-like breast cancer. *Proc Natl Acad Sci USA* 104: 12111 – 12116

Menzies A, Teague JW, Butler AP, Davies H, Tarpey P, Nik-Zainal S, Campbell PJ (2015) VAGrENT: variation annotation generator. *Curr Protoc Bioinformatics* 52: 15.8.1 – 15.8.11

Nik-Zainal S, Davies H, Staaf J, Ramakrishna M, Glodzik D, Zou X, Martincorena I, Alexandrov LB, Martin S, Wedge DC *et al* (2016) Landscape of somatic mutations in 560 breast cancer whole-genome sequences. *Nature* 534: 47 – 54

Nishimasu H, Shi X, Ishiguro S, Gao L, Hirano S, Okazaki S, Noda T, Abudayyeh OO, Gootenberg JS, Mori H *et al* (2018) Engineered CRISPR-Cas9 nuclease with expanded targeting space. *Science* 361: 1259 – 1262

Raine KM, Hinton J, Butler AP, Teague JW, Davies H, Tarpey P, Nik-Zainal S, Campbell PJ (2015) cgpPindel: Identifying somatically acquired insertion and deletion events from paired end sequencing. *Curr Protoc Bioinformatics* 52: 15.7.1 – 15.7.12

Rees HA, Liu DR (2018) Base editing: precision chemistry on the genome and transcriptome of living cells. *Nat Rev Genet* 19: 770 – 788

Robinson MD, McCarthy DJ, Smyth GK (2010) edgeR: a Bioconductor package for differential expression analysis of digital gene expression data. *Bioinformatics* 26: 139 – 140

Rottenberg S, Pajic M, Jonkers J (2010) Studying drug resistance using genetically engineered mouse models for breast cancer. *Methods Mol Biol* 596: 33 – 45

Sanjana NE, Shalem O, Zhang F (2014) Improved vectors and genome-wide libraries for CRISPR screening. *Nat Methods* 11: 783 – 784

Tan J, Zhang F, Karcher D, Bock R (2019) Engineering of high-precision base editors for site-specific single nucleotide replacement. *Nat Commun* 10: 439

Thuronyi BW, Koblan LW, Levy JM, Yeh WH, Zheng C, Newby GA, Wilson C, Bhaumik M, Shubina-Oleinik O, Holt JR *et al* (2019) Continuous evolution of base editors with expanded target compatibility and improved activity. *Nat Biotechnol* 37: 1070 – 1079

Zafra MP, Schatoff EM, Katti A, Foronda M, Breinig M, Schweitzer AY, Simon A, Han T, Goswami S, Montgomery E *et al* (2018) Optimized base editors enable efficient editing in cells, organoids and mice. *Nat Biotechnol* 36: 888 – 893

Zuo E, Sun Y, Wei W, Yuan T, Ying W, Sun H, Yuan L, Steinmetz LM, Li Y, Yang H (2019) Cytosine base editor generates substantial off-target single-nucleotide variants in mouse embryos. *Science* 364: 289 – 292

© 2020 The Authors